Downloaded from orbit.dtu.dk on: May 01, 2024

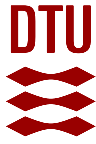

DTU Library

Membrane dynamics of γ-secretase with the anterior pharynx-defective 1B subunit

Dehury, Budheswar; Kepp, Kasper Planeta

Published in:
Journal of Cellular Biochemistry

Link to article, DOI:
10.1002/jcb.29832

Publication date:
2021

Document Version
Peer reviewed version

Link back to DTU Orbit

Citation (APA):
Dehury, B., & Kepp, K. P. (2021). Membrane dynamics of γ-secretase with the anterior pharynx-defective 1B subunit. *Journal of Cellular Biochemistry*, *122*(1), 69-85. https://doi.org/10.1002/jcb.29832

General rights
Copyright and moral rights for the publications made accessible in the public portal are retained by the authors and/or other copyright owners and it is a condition of accessing publications that users recognise and abide by the legal requirements associated with these rights.

- Users may download and print one copy of any publication from the public portal for the purpose of private study or research.
- You may not further distribute the material or use it for any profit-making activity or commercial gain
- You may freely distribute the URL identifying the publication in the public portal

If you believe that this document breaches copyright please contact us providing details, and we will remove access to the work immediately and investigate your claim.

Membrane Dynamics of γ-Secretase with the Anterior Pharynx-Defective 1B Subunit

Budheswar Dehury and Kasper P. Kepp*

Technical University of Denmark, DTU Chemistry, DK-2800 Kongens Lyngby, Denmark

* Corresponding author. E-mail: kpj@kemi.dtu.dk; Phone: +45-45252409

RUNNING TITLE: γ-Secretase with the Anterior Pharynx-Defective 1B

ORCID:

Budheswar Dehury: 0000-0002-9726-8454

Kasper P. Kepp: 0000-0002-6754-7348

Acknowledgements

The authors acknowledge computational resources from DTU High-Performance Computing (HPC) facility, Lyngby, DTU. The Novo Nordisk Foundation, grant NNF17OC0028860, is gratefully acknowledged for supporting this work.

27 **Abstract**

28 The four-subunit protease complex γ-secretase cleaves many single-pass transmembrane
29 substrates, including Notch and β-amyloid precursor protein to generate Aβ, central to
30 Alzheimer's disease. Two of the subunits, anterior pharynx-defective 1 (APH1) and presenilin
31 (PS), exist in two homologous forms, APH1-A and APH1-B, and PS1 and PS2. The
32 consequences of these variations are poorly understood and could affect Aβ production and γ-
33 secretase medicine. Here, we developed the first complete structural model of the APH-1B
34 subunit using the published cryo-EM structures of APH1-A (PDB: 5FN2, 5A63 and 6IYC).
35 We then performed all-atom molecular dynamics simulations at 303 K in a realistic bilayer
36 system to understand both APH-1B alone and in γ-secretase without and with substrate C83
37 bound. We show that APH-1B adopts a 7TM topology with a water channel topology similar to
38 APH-1A. We demonstrate direct transport of water through this channel, mainly via Glu84,
39 Arg87, His170, and His196. The apo and holo states closely resemble the experimental cryo-
40 EM structures with APH-1A, however with subtle differences: The substrate-bound APH-1B-
41 γ-secretase was quite stable, but some TM helices of PS1 and APH-1B rearranged in the
42 membrane consistent with the disorder seen in the cryo-EM data. This produces different
43 accessibility of water molecules for the catalytic aspartates of PS1, critical for Aβ production.
44 In particular, we find that the typical distance between the catalytic aspartates of PS1 and the
45 C83 cleavage sites are shorter in APH-1B, i.e. it represents a more closed state, due to
46 interactions with the C-terminal fragment of PS1. Our structural-dynamic model of APH-1B
47 alone and in γ-secretase suggests generally similar topology but some notable differences in
48 water accessibility which may be relevant to the protein's existence in two forms and their
49 specific function and location.

50

51 **Keywords:** γ-secretase; Alzheimer's disease; APH1-B; molecular dynamics, membrane
52 protein

53 **Introduction**

54 Alzheimer's disease (AD), the major neurodegenerative disease that affects tens of millions of
55 people worldwide and causes gradual impairment of memory, cognition, and identify, is linked
56 to deposits of aggregated amyloid-β peptides (Aβ) in senile plaques.[Blennow et al., 2015;
57 Selkoe and Hardy, 2016] The Aβ peptides are formed by cleavage of the β-amyloid precursor
58 protein (APP) by β-secretase, giving first the C99 fragment, and then γ-secretase, giving Aβ
59 peptides of different lengths.[Esch et al., 1990; Golde et al., 1992; Julia and Goate, 2017;
60 Takami et al., 2009; Vassar et al., 1999] Of the two most predominant isoforms, the shorter 40-
61 residue $A\beta_{40}$ has natural functions[Kepp, 2017; Lee et al., 2004a; Smith et al., 2002] and is less
62 toxic than $A\beta_{42}$, which has two more hydrophobic residues, often forms oligomers and
63 aggregates.[Cheung et al., 2006; Hardy and Higgins, 1992] and could be a molecular culprit of
64 AD.[Sun et al., 2016; Tang and Kepp, 2018]

65 γ-secretase is an integral membrane aspartyl protease complex comprised of four discrete
66 protein subunits, nicastrin, presenilin (PS1/PS2), anterior pharynx-defective 1 (APH-1A/B),
67 and presenilin enhancer 2 (PEN-2)[Kimberly et al., 2003; Sato et al., 2007]. The membrane
68 protease is a major player in membrane protein turnover as it catalyzes intramembrane
69 hydrolysis of more than 100 single-pass TM substrates with diverse cellular
70 functions.[Haapasalo and Kovacs, 2011] Mutations in the catalytic subunit PS1/PS2 and in the
71 substrate APP are the main causes of early-onset familial AD, suggesting that disease somehow
72 correlates with changes in APP processing.[Luukkainen et al., 2019] Most of these mutations
73 tend to lower enzyme activity and increase the ratio of formed $A\beta_{42}/A\beta_{40}$, a tendency that
74 significantly correlates with the clinical onset of the disease in mutation carriers.[Sun et al.,
75 2016; Tang and Kepp, 2018] This ratio could cause disease either by toxic gain of function of
76 $A\beta_{42}$[Cheung et al., 2006; Hardy and Higgins, 1992; Pauwels et al., 2012] or by loss of natural
77 function of $A\beta_{40}$[Kepp, 2016] or other substrates of γ-secretase.[Shen and Kelleher, 2007] For
78 these reasons, the processing efficiency of γ-secretase is central to understanding AD and

79 therapeutic efforts to modulate it are ongoing.[Crump et al., 2013; Golde et al., 2013; Imbimbo
80 and Giardina, 2011]

81 Among the subunits of γ-secretase, APH-1 is a 7TM protein that aids the trafficking and
82 assembly of the enzyme complex.[Francis et al., 2002; Goutte et al., 2002; Sun et al., 2015] In
83 humans, APH-1 is encoded by two homologous genes APH-1A and APH-1B, and APH-1A
84 includes two alternatively spliced transcripts forming APH-1A(L-large) and APH-1A(S-
85 small).[Gu et al., 2003; Lee et al., 2002] APH-1A and APH-1B associate with PS1/2, NCT and
86 PEN-2 to produce active γ-secretase complexes with diverse biochemical and physiological
87 properties and locations.[Araki et al., 2006; Serneels et al., 2009; Shirotani et al., 2004] Despite
88 this heterogeneity, all structural studies and most biochemical studies have so far concentrated
89 on APH-1A as the preferred model of γ-secretase and Aβ production. Understanding how
90 APH-1B affects the structure, dynamics and function of the complex is thus of substantial
91 interest.

92 APH-1A has been suggested to form a water channel of the membrane-bound enzyme
93 complex, but whether APH-1B does the same is unknown.[Aguayo-Ortiz and Dominguez,
94 2019] APH-1B γ-secretase seems to play a special role in processing of the membrane-bound
95 signaling molecule neuregulin-1(NRG-1).[Dejaegere et al., 2008; Fazzari et al., 2014]
96 Inactivation of APH-1B-γ-secretase in a mouse AD model may improve some AD-related
97 features without any Notch-related side effects,[Serneels et al., 2009] whereas low expression
98 of APH-1B may cause neurodevelopmental phenotypes in rats.[Coolen et al., 2006]
99 Importantly, APH-1B has been reported to increase the $A\beta_{42}/A\beta_{40}$ ratio without modifying ε-
100 cleavage position.[Lessard et al., 2015] These various studies suggest that APH-1B does not
101 work identically to APH-1A in the protein complex.

102 With the advancements in cryogenic-electron microscopy (Cryo-EM) structures, γ-
103 secretase has been characterized at near atomic resolution in both the apo state (PDB: 5A63,
104 5FN2, 5FN3, 5FN4 and 5FN5) and as substrate-bound holo states (6IYC and 6IDF).[Bai et al.,

2015b, 2015a; Sun et al., 2015; Yang et al., 2019; Zhou et al., 2019] These structures have opened new avenues for a mechanistic understanding of AD. All of these structures involve the APH-1A subunit, APH-1B not yet structurally characterized. We also note that the cryo-EM structures represent compositions on a film, which structurally resemble a mixture of the states in lipid and water, whereas the real protein complex acts dynamically at physiological temperature in a complete membrane. Both the membrane and the temperature work together to expand the protein's conformation states, as recently shown by direct comparison of the experimental and simulated ensembles at high and low temperature, and with and without membrane.[Mehra et al., 2020] Molecular dynamics (MD) simulations are thus essential to understand the physiological temperature dynamics of this important protein complex in realistic membrane models on the background of the experimental structural constraints, as now intensely pursued in several dedicated computational chemistry labs.[Aguayo-Ortiz et al., 2018; Aguayo-Ortiz and Dominguez, 2018; Dehury et al., 2019a, 2019b, 2019c; Dominguez et al., 2016; Hitzenberger and Zacharias, 2019a; Kong et al., 2015; Mehra et al., 2020; Petit et al., 2019; Somavarapu and Kepp, 2017]

We present here the first structural models, obtained from homology modeling, of both APH-1B alone and APH-1B-γ-secretase in both the apo- and substrate-bound states. These structural models were then embedded in complete water-bilayer systems and studied in triplicate by all-atom MD simulations. To the best of our knowledge, this is the first study of the structure and dynamics of APH-1B both alone and inside γ-secretase. Our study notably identifies the conformational dynamics of γ-secretase with APH-1B inside a realistic membrane model at relevant temperature, identifies a water conductance channel in the structures, and quantifies several different conformational states of APH-1B-γ-secretase as compared to the APH-1A isoform.

131 **Computational methods**

132

133 **Molecular Modeling of APH-1B alone**

134 The three-dimensional structure of APH-1B subunit is not known. However, APH-1A and
135 APH-1B (257 amino acids, UniProtKB ID: Q8WW43) share ~57% sequence identity. To
136 model APH-1B, we used BLASTp[Altschul et al., 1997] to search for experimental protein
137 structures in the protein data bank (PDB) as optimal templates for homology modeling. As
138 expected, BLAST suggested the cryo-EM structures of γ-secretase APH-1A subunits (5FN2,
139 5A63 and 6IYC) as the most reliable templates with high query coverage. The templates
140 feature the same APH-1A subunit and very similar topology (Cα-RMSD of 0.32 Å
141 (5FN2/5A63), 0.59 Å (5A63/6IYC), and 0.67 Å (5FN2/6IYC). We used the evaluation criteria
142 of Modeller version 9.23[Webb and Sali, 2017] to characterize the structures by their least
143 discrete optimized protein energy (DOPE). The structures were then optimized using the loop
144 model protocol in Modeller and the Galaxy refine tool.[Heo et al., 2013] The model with least
145 Cα-RMSD vs. the templates was selected and validated by SAVES version 5.0
146 (https://servicesn.mbi.ucla.edu/SAVES/) and Molprobity.[Chen et al., 2010] Based on the
147 model validation statistics (**Table S1**), APH-1B structures used to build different forms of γ-
148 secretase were chosen as described in further detail below.

149

150

151 **Constructing a model of γ-secretase with APH-1B subunit**

152 We developed four systems for all-atom molecular dynamics simulation i.e., one of APH-1B
153 alone in a membrane and three γ-secretase states with APH-1B in a membrane (apo-state with
154 both catalytic aspartates deprotonated, apo-state with protonated Asp-257, and C83-bound).

155 For the apo state, we used the cryo-EM structure of γ-secretase resolved at 4.2 Å resolution
156 (PDB ID: 5FN2) as the initial template.[Bai et al., 2015a] The missing side-chains of the

157 structure were built using the WHAT-IF server.[Hekkelman et al., 2010] The long intracellular
158 loop 2 (264 to 377 amino acids of PS1) bridging TM6 and TM7 of the PS1 component was not
159 included due to the lack of available structural information; since we are mainly interested in
160 APH-1A/1B differences, the absence of these structural data in PS1 should be less critical to
161 our work. Then the complete γ-secretase model was developed upon structural superposition
162 and coordinate transfer of each subunit using PyMOL version 2.0, (The PyMOL Molecular
163 Graphics System, Version 2.0 Schrödinger, LLC.), replacing APH-1A with our modeled APH-
164 1B subunit. was The APH-1B-γ-secretase complex was then embedded in a POPC bilayer
165 using CHARMM36m.[Huang et al., 2016].

166 We simulated two distinct γ-secretase models (apo forms), one with both catalytic residues
167 (Asp257 and Asp385 of PS1) deprotonated, and the other with protonated Asp257. Previous
168 pK_a calculations of both experimental and simulated structures have shown that these are the
169 only likely protonation states, with deprotonation being most prevalent at neutral pH.[Mehra et
170 al., 2020] BIOVIA Discovery Studio Visualizer (Dassault Systèmes BIOVIA, BIOVIA DSV,
171 4.5, San Diego: Dassault Systèmes, 2019) was used to remove steric clashes before merging
172 the model with the membrane-solvent system. The arrangement of γ-secretase with respect to
173 the lipid bilayer was obtained from the Orientation of Proteins in Membranes (OPM)
174 server.[Lomize et al., 2012] For the substrate-bound model, the initial 3D coordinates were
175 adopted from 6IYC.[Zhou et al., 2019] After removal of hetero-atoms, the mutations Q112C
176 and D385A in the catalytic subunit PS1 were converted to the wild type using PyMOL, as these
177 are necessary artifacts of the experimental protocol required to keep the substrate inside the
178 protein.

179

180 **MD simulations**

181 The atomic details and compositions of all the studied systems are summarized in **Table S2**.
182 We used the CHARMM-GUI membrane builder[Jo et al., 2008] to insert the proteins into a

hydrated, equilibrated bilayer composed of 2-oleoyl-1-palmitoyl-sn-glycero-3-phosphocholine (POPC) molecules in the upper and lower leaflet. Sodium and chloride ions were added to neutralize the system, reaching a final concentration of approximately 150 mM. Each of the above-described systems were simulated by three independent MD simulations of 500 ns using GROMACS version 2018.5[Abraham et al., 2015] applying the CHARMM36m force field and the TIP3P water model. The input systems were first subjected to energy minimization, equilibration, and then production simulation using the GROMACS input scripts generated by the CHARMM-GUI. Each system was energy minimized using 5,000 steps of steepest descent, followed by 1 ns of NVT (constant particle number, volume, and temperature) and NPT (constant particle number, pressure, and temperature) equilibrations. The van der Waals interactions were evaluated using a switching cutoff at 10–12 Å, whereas the long-range electrostatic interactions were calculated using the particle-mesh Ewald procedure. The temperature and pressure were held at 303.15 K and 1 bar, respectively.

During the production simulations, an NPT ensemble was used with semi-isotropic pressure coupling via the Parrinello–Rahman barostat method, whereas the Nose–Hoover thermostat was used to maintain a temperature of 303.15 K. A leapfrog integration scheme was used, and all covalent bonds were constrained. We used a time-step of 2 ps during both NPT equilibration and production MD simulations.

Analysis of MD Trajectories

All simulations were analyzed using the inbuilt GROMACS tools and FATSLiM tools.[Buchoux, 2017] The 2-dimensional plots were generated with XMGRACE (http://plasma-gate.weizmann.ac.il/Grace/), whereas structures were rendered using PyMOL. Deuterium order parameters, the density of the membrane components, and the area per lipid head group were computed using FATSLiM. Principal component analysis (PCA) was employed to identify the large-scale collective motions of main-chain atoms of each system

209 using the last 300 ns trajectories of each simulation, since equilibration typically takes 1-200 ns
210 for these large membrane-embedded protein complexes, i.e. the first 1-200 ns may contain
211 artefacts of the non-equilibrated starting models.[Dehury et al., 2019b; Somavarapu and Kepp,
212 2017] Clustering analysis was performed with the *gmx cluster* utility toolkit and a cut-off of 0.2
213 nm to select the most representative structures of each simulated ensemble, using the last 300
214 ns of each trajectory.
215

216 **Results and discussion**

217

218 **Sequence and structure differences between APH-1A and APH-1B**

219 Pair-wise sequence alignment using MultAlin (**Figure 1A**) shows that APH-1A and APH-1B
220 share 75% sequence similarity and 57% identity. The N-terminal is more conserved than the C-
221 terminal, and there are variations in the loops connecting the TM segments. As described in
222 methods, we used the APH-1A structures solved by cryo-EM (5FN2, 5A63 and 6IYC) as
223 templates to construct a complete model of the human APH-1B subunit. Based on
224 Procheck[Laskowski et al., 1993], 97.8% (221) of the residues of our model were in the most
225 favored regions and 2.2% (5 residues) were in additional favored regions, with no residues in
226 disallowed regions of the Ramachandran plot (**Figure 1B**), indicating the high quality of our
227 proposed model. These results were confirmed by Molprobity[Chen et al., 2010], giving 99.2%
228 residues in favored regions with no residues having poorly described rotamers and bonds.
229 Similarly, 81.4% of the residues had 3D-1D scores > 0.2 as calculated by Verify 3D,[Lüthy et
230 al., 1992] and the overall quality score of 94.6 from ERRAT[Colovos and Yeates, 1993] shows
231 that the modeled structure is very realistic by any of the normal structural assessment
232 standards.

233 The 7TM helical topological architecture of our modelled APH-1B with conserved (red)
234 and variable (white) regions is shown in **Figure 1C**. The Gly122, Gly126, and Gly130 residues
235 (**Figure 1A** and **1D**) in TM4 constitute a part of the membrane GxxxG motif, which is essential
236 for stable association of APH-1A(L) with the other subunits by helix-helix interactions and
237 highly conserved.[Araki et al., 2006; Lee et al., 2004b] Structural superimposition of our APH-
238 1B model with APH-1A from 5FN2, 5A63, and 6IYC (**Figure 1D**) gave Cα-RMSD values of
239 0.47, 0.37, and 0.46 Å, respectively, i.e. our proposed model fully respects the structural
240 constraints from the experimental structures. There are some minor differences in the loops
241 bridging the TMs **(Figure 1D)** as expected from the different sequences (**Figure 1A**). Whether

242 these differences become more pronounced upon full equilibration of the model by MD is
243 analyzed below.
244

245 **All-atom dynamics of APH-1B in a realistic membrane structure**

246 Since APH-1B as well as γ-secretase are membrane proteins, understanding their structures and
247 dynamics in the context of a membrane is essential, with membrane proteins typically adopting
248 distinct conformational states in membranes that may contribute to protein activity.[Corradi et
249 al., 2019; Zhuang et al., 2014, 2016] Our APH-1B systems were comprised of 240 POPC
250 lipids, 18,611 water molecules, and 49 Na^+ and 56 Cl^- ions. In order to assess whether our
251 protein-lipid-water system is realistic, we computed various membrane properties, including
252 the deuterium order parameters, the local density of the membrane components, and the
253 distribution of area per lipid for each system (**Figure S1** and **S2**). The computed membrane
254 order parameters compare excellently with the experimental data for equivalent protein-
255 membrane systems.[Zhuang et al., 2016] In particular, the deuterium order parameters with the
256 splitting near the lipid head-group closely resemble experimental values. Artificial changes in
257 the simulated membrane structure would be revealed from the density profiles, but our values
258 are close to experiment, indicating that the overall membrane structure integrity is maintained
259 (**Figure S1**). The average lipid per unit area of ~0.62 nm resembles that expected for
260 CHARMM36m simulations.[Lyubartsev and Rabinovich, 2016]

261 The dynamical stability of our systems were monitored by computing the backbone RMSD
262 relative to the starting structure across the full 500 ns of each triplicate simulation, as shown in
263 **Figure 2A**. The systems reached stable conformational ensembles after ~150 ns and
264 maintained a horizontal trend with an average RMSD of ~2.8−3.2 Å. The variation in RMSD
265 implies somewhat different conformational states of APH-1B being sampled, as explored
266 further below. The root-mean square fluctuations (RMSF) of each Cα-atom of APH-1B
267 averaged over the trajectories are displayed in **Figure 2B**. The TMs (3-26: TM1, 31-57: TM2,

268 65-104: TM3, 113-138: TM4, 156-183: TM5, 186-204: TM6 and 213-229: TM7) displayed
269 reduced flexibility, enforced further by their embedding in the membrane, whereas the loops
270 bridging TM2 -TM3 and TM4-TM5 were highly flexible. We note the general very good
271 agreement between the three independent simulations indicating that the obtained dynamics of
272 APH-1B are reproducible and significant.

273 To ensure that the simulated structures remain realistic, we compared the most
274 representative ensemble structures from cluster analysis to the experimental APH-1A structure
275 (5FN2) (**Figure 2C**). The Cα-RMSD values of 2.54, 2.17 and 1.97 Å are very reasonable since
276 our model represents free APH-1B alone in a membrane, whereas the experimental structure
277 represents APH-1A in the γ-secretase in a chemical composition somewhere between water
278 and a lipid system, on a sample film. The APH-1B loops are dynamic, as expected.

279

280 **Active water channel in APH-1B**

281 The electrostatic surface potential for the experimental APH-1A (5FN2) and for our three
282 ensemble-representative APH-1B structures (**Figure S3**) indicates different charge
283 distributions near TM5 and adjacent loops. A large cavity is formed adjacent to TM2 and TM3,
284 which may be due to the flexibility of the loops in C-terminal TM segments. The obtained
285 cavities with variable interior space resemble different states of a membrane solvent channel,
286 with indications of both an open and more closed structure (**Figure S3**).

287 To understand the obtained APH-1B ensemble better, we performed PCA on the last 300
288 ns of each trajectory, with the eigenvalues of first two eigenvectors (EVs) and the projection of
289 the movements of main-chain atoms summarized in **Figure S4A-S4B**. Simulation 1 (blue)
290 represents a more open conformational ensemble, whereas simulation 2 (red) is in-between and
291 simulation 3 is the least variable (most compact) state. To understand these variations, we
292 generated porcupine plots for top EVs containing the major movements (**Figure S4C**).
293 Consistent with the RMSF analysis, most TMs were rigid, and the loop bridging TM4-TM5

294 was flexible. We also identify a significant inward motion of the C-terminal of TM2 and N-
295 terminal of TM3, (these two TMs are somewhat separated from the remaining TMs), which
296 correlates with the opening and closing of the cavity in the membrane.

297 We note that the cryo-EM structure of the APH-1A subunit within γ-secretase (PDB: 5FN3
298 solved at 4.1 Å) already indicates a central cavity similar to small molecule/ligand recognition
299 sites in G-protein coupled receptors (GPCR).[Sun et al., 2015] In addition, a recent study has
300 shown that the central region of APH-1A (mostly occupied by TM3) possesses lower
301 hydropathy due to the polar residues in the cavity.[Aguayo-Ortiz et al., 2018] Our obtained
302 APH-1B cavities are thus not unusual, yet manifest very clearly. Crystallographic GPCR
303 structures and MD simulations indicate that the polar central cavity enables entry of water
304 molecules into the membrane, which is usually excluded.[Lee et al., 2016] These water
305 molecules play important regulatory and activation roles in GPCRs.[Angel et al., 2009] To
306 understand if this is the case also for APH-1B, we inspected our ensemble-representative
307 structures and identified multiple water-containing sites within the membrane/TM region. As
308 for GPCRs, we find that the water-containing cavity of APH-1B crosses the middle part of the
309 membrane and almost reaches the intracellular space. It is well-known that water influx into
310 GPCR central cavities allows the occasional transport of water molecules from one cellular
311 compartment to another[Lee et al., 2016; Tomobe et al., 2017] and we thus consider this
312 analogy for APH-1B to be of interest.

313 More specifically, we found that a variable number (average ~37) of water molecules
314 crossed APH-1B and formed a continuous water channel within the membrane-protein system
315 (**Figure S5** and **S6**). We observed multiple events of complete transfer of water molecules at
316 the studied time scale (200−500 ns) both from the extracellular to the intracellular space and
317 vice-versa. Close inspection of the MD snapshots revealed that TM3, TM4, TM5, and TM6
318 interact with the water molecules during translocation (**Figures S5-S6**). The water molecules
319 interacted particularly with the polar residues Glu84, Arg87, His170, and His196. Interestingly,

320 both APH-1A and APH-1B harbors strongly conserved histidines His170 and His196, which is
321 consistent with a possible conversed role in water transportation across the bilayer.

322 A water channel is likely to be regulated by conformational changes of the membrane-
323 protein system. To understand such effects, we monitored the dynamic changes in the helix tilt
324 angles of TM2, TM4, TM5 and TM6, which were found to vary considerably (**Figure S7**).
325 Since lipid headgroups play a vital role in membrane protein function,[Bogdanov et al., 2008]
326 we analyzed the APH-1B residues that consistently formed hydrogen bonds with the POPC
327 headgroups (**Figure S8**). We observed that positively charged arginine and lysine as well as
328 cysteine at the cytoplasmic edge of the TM helices hydrogen bonded with the headgroups.

329

330 **Dynamics of γ-Secretase complex with APH-1B**

331 Whereas the results above concerned the free APH-1B in a membrane, in the following we
332 discuss our analogous results for the complete APH-1B-γ-secretase system. The structure,
333 stability, and functions of a membrane protein depend on its orientation in the membrane, the
334 spatial distribution of amino acid residues within the membrane protein, and the lipid
335 composition.[Bondar and White, 2012; Lomize et al., 2006, 2012; Ng et al., 2014] This also
336 applies to γ-secretase, whose lipid environment is known to affect the biological
337 activity.[Aguayo-Ortiz et al., 2018] γ-secretase tends to remain active in a membrane
338 composed solely of phosphatidylcholine (PC) lipids, but the substrate cleavage activity is
339 modulated by the membrane structure and composition.[Osenkowski et al., 2008] Thicker
340 membranes favor the production of $A\beta_{40}$, while thinner membranes favor $A\beta_{42}$
341 production,[Osenkowski et al., 2008; Winkler et al., 2012] in good agreement with the Fit-
342 Induce-Stay-Trim (FIST) model, where more compact, hydrophobic, tight "grapping" of the
343 substrate in the semi-open state, controlled by TM2, TM3, TM6, and TM9 of PS1, leads to
344 stabilized enzyme-substrate interactions, longer retention and extended cleavage of C99 to
345 shorter Aβ.[Somavarapu and Kepp, 2016, 2017] Accordingly, more carbons in the lipid chains

346 increase the activity of γ-secretase and reduce the $A\beta_{42}/A\beta_{40}$ ratio,[Holmes et al., 2012] which
347 correlates with the clinical onset of familial AD.[Sun et al., 2016; Tang and Kepp, 2018]

348 For these reasons, the ambient temperature dynamics in a realistic membrane model, as
349 can be obtained from MD simulations, are thus an important supplement to the cryo-EM
350 structural data needed to understand the structure-dynamics-function relations, in particular in
351 relation to substrate binding and cleavage of C83 to produce Aβ.[Mehra et al., 2020]

352 To ensure that the complex membrane-water-protein ensembles are realistically described,
353 we computed the order parameters (S_{cd}), membrane properties, area per lipid distribution of the
354 sampled lipid bilayers as a necessary first quality control (**Figure S9** and **S10**). All properties
355 were in agreement with experimental membrane properties and MD simulations of equivalent
356 membrane-protein systems.[Zhuang et al., 2014, 2016] Thus, we have produced a realistic high
357 quality model of APH-1B not only in close structural agreement with the cryo-EM data for
358 APH-1B, but also with a realistic membrane system. This model is the first of APH-1B-γ-
359 secretase to our knowledge.

360 **Figure 3** displays the backbone RMSD values for the simulated γ-secretase systems. The
361 backbone RMSD of APH-1B-apo-γ-secretase with deprotonated Asp257 and Asp385 increased
362 until 200 ns but then stabilized and averaged ~3.5 Å for the three independent simulations
363 (**Figure 3A**). The RMSD of apo-γ-secretase with protonated Asp257 averaged to ~3.8 Å for
364 the three simulations (**Figure 3B;** simulation 2 had a distinct compact state). In contrast, the
365 C83-bound APH-1B-γ-secretase was consistently less variable (**Figure 3C**). After ~150 ns,
366 both the apo and holo-states displayed stable evolution, and the RMSD remained close to the
367 experimental structures 5FN2 (RMSD < 4 Å) and 6IYC (RMSD < 3 Å), in agreement with
368 previous simulations of APH-1A-apo-γ-secretase[Somavarapu and Kepp, 2017] and C99-
369 bound APH-1A-γ-secretase[Dehury et al., 2019b]. The RMSD of each subunit (**Figure S11**)
370 shows that nicastrin displayed higher RMSD typical of the large inward-outward movement
371 relative to the membrane as reported in many other studies.[Aguayo-Ortiz et al., 2017;

372 Aguayo-Ortiz and Dominguez, 2018; Bai et al., 2015a; Somavarapu and Kepp, 2017] PEN2
373 varied in its conformation space for the apo- and holo-states, consistent with an rearrangement
374 of PS1 upon substrate binding already evident from the cryo-EM data.[Zhou et al., 2019] Other
375 subunits displayed stable ensembles after 200 ns, and APH-1B was clearly less structurally
376 variable in the C83-bound state, i.e. substrate binding dampens APH-1B dynamics. The radius
377 of gyration (R_g) and solvent accessible surface area (SASA), which monitor the shape and
378 compactness of the ensembles (**Figure S12**), were largely constant with minor changes during
379 the initial 200 ns. The obtained R_g values were 39.6−40.2 Å for the apo-γ-secretase systems
380 and 39.9−40.6 Å for the substrate-bound state.

381 To compare our structures quantitatively with the experimental cryo-EM structures for
382 APH-1A-γ-secretase, we extracted the top-ranked structure from cluster analysis of the last 300
383 ns of each simulated trajectory (**Figure S13**) and structurally aligned the Cα-atoms of these
384 structures with those of the cryo-EM structures for apo-γ-secretase (5FN2[Bai et al., 2015a]
385 with APH-1A) system, the RMSD values were 2.54, 2.17 and 1.97 Å for the triplicate
386 simulations (**Figure S13A)**. Apo-γ-secretase with protonated Asp257 gave 2.43, 3.68, and 2.46
387 Å, respectively (**Figure S13B)**; the large value of 3.68 Å arose from an open PS1/PS2 state as
388 seen previously[Dehury et al., 2019b, 2019a; Somavarapu and Kepp, 2017]. C83-bound APH-
389 1B-γ-secretase compared to 6IYC[Zhou et al., 2019] gave RMSD values of 1.81, 2.32, and
390 1.37 Å (**Figure S13C)**. Considering the resolution of the cryo-EM structures (5FN2: 4.2 Å and
391 6IYC: 2.6 Å), our MD simulated models thus obey the experimental topology and provide an
392 accurate basis for exploring the all-atom membrane-protein dynamics at physiological
393 temperature.

394 We compared the representative ensemble structures from clustering analysis with the
395 experimental apo (5FN2) and holo (6IYC) states (**Figure 4**). We observed complete loss of β-
396 strand of C83 in all systems, consistent with findings that this strand is lost in membranes at
397 normal temperature but prevails at low temperature.[Mehra et al., 2020] In one simulation, we

398 observed retention of the two β-strands in PS1 (one extended from TM6 and the other with
399 TM7). In other systems, both these strands were converted to turns, indicating that they are
400 mostly flexible and undergo coil-turn-strand transitions at ambient temperature, as shown
401 previously.[Mehra et al., 2020] Close inspection of the APH-1B subunit as compared to APH-
402 1A revealed that the TM regions are essentially similar except for the small C-terminal JM
403 helix. Furthermore, we observed minor differences in the arrangement of TM helices in APH-
404 1B probably due to the sequence-distinct loops connecting these TMs (**Figure 1A**).
405

406 **Residue-specific dynamics of γ-secretase with APH-1B**

407 To understand the residue-wise dynamics, we plotted the Cα root-mean-squared forces
408 (RMSF), which resemble qualitatively (but not quantitatively[Caldararu et al., 2019])
409 crystallographic B-factors[Sun et al., 2019], for each subunit of the complexes (**Figure 5**). As
410 anticipated, the RMSF of nicastrin-ECD displayed numerous high peaks as typical of loops,
411 while the TM helix (Ser665−Phe698) was distinctly rigid. The extracellular residues of
412 nicastrin Phe240−Glu245 probably contribute to substrate recognition[Petit et al., 2019] and to
413 the dynamic stability of γ-secretase-Aβ assemblies.[Szaruga et al., 2017] In the C83-bound
414 holo enzyme, we observed very little fluctuations in this region as compared to both the apo
415 systems. The extra-cellular hydrophilic loop 1 (HL1) bridging TM1 and TM2 in PS1,
416 potentially involved in substrate gating,[Takagi-Niidome et al., 2015] displayed notably
417 differential fluctuations in the apo and holo states. HL1 also constitutes a binding pocket for γ-
418 secretase modulators[Cai et al., 2017] which may thereby affect differently the apo and
419 substrate-bound state.[Zhou et al., 2019]

420 We observed large movements of the N-terminal of TM2 and TM9, in good agreement
421 with our previous findings.[Dehury et al., 2019b; Somavarapu and Kepp, 2017] The APH-1B
422 and PEN2 subunits displayed more or less the same trends in RMSF for the apo and holo
423 states. The dynamics properties of the substrate C83 have been illustrated in **Figure S14**. The

424 hydrophilic loop 2 (HL2) bridging TM6 and TM7 is missing in the experimental apo structures
425 and in the present models, whereas the C83-bound conformation harbors two β-strands in PS1,
426 β1 comprised of Ile287−Tyr288−Ser289 extended from TM6a, and β2 involving five residues
427 of TM7 (Gly378−Gly382). The C-terminal fragment of C83 harbors the TM helix and a β-
428 strand Val721−Lys725, which displayed very distinct fluctuation in one simulation (**Figure**
429 **S14B**). This fluctuation correlated with a loose conformation of C83 inside γ-secretase, i.e. the
430 pathogenic "open" state of PS1 that produces less active, imprecise cleavage and longer Aβ
431 peptides according to the FIST model.[Dehury et al., 2019b; Somavarapu and Kepp, 2017;
432 Tang et al., 2018]
433

434 **Characterizing the ensembles by principal component analysis**

435 To capture global motions in various γ-secretase complex systems we performed PCA on the
436 last 300 ns of each trajectory (**Figure S15-S17**). The most pronounced motions depicted by the
437 top eigenvectors (**Figure S16-S17**) quantify the large breathing mode of the nicastrin ECD in
438 both the apo- and holo-states. The second principal component (**Figure S17**) indicated a
439 different but correlated opening and closing motion that changes the size of the cavity formed
440 by the nicastrin ECD and the TMDs, in good agreement with previous studies.[Aguayo-Ortiz et
441 al., 2017; Elad et al., 2015; Lee et al., 2017] This motion is probably responsible for the
442 guiding of substrate molecules towards the intramembrane cleavage site of γ-
443 secretase.[Fukumori and Steiner, 2016]

444 Additional dynamics were observed in the TM helices of PS1, with TM2 and the directly
445 connected N-terminal region of TM3 being highly mobile in both apo and substrate bound
446 states (**Figure S16** and **S17**). These dynamic motions largely explain the static low resolution
447 (disorder) in the experimental cryo-EM structures 5FN2[Bai et al., 2015a] and 6IYC[Zhou et
448 al., 2019], and has been repeatedly found by MD simulations.[Dehury et al., 2019a, 2019b,

449 2019c; Mehra et al., 2020; Somavarapu and Kepp, 2017] We also note that the loops in C-
450 terminal region of APH-1B displayed some movements in all the studied γ-secretase states.
451 To better understand the two major motions of the two nicastrin ECD lobes relative to PS1
452 in apo and holo γ-secretase, we measured the distances and angles formed between amino acids
453 Leu121 (small lobe), Val328 (large lobe) of ECD and the active site residue Asp257 of PS1
454 (**Figure S18** and **Table S3**). The Val328−Asp257 distances differed significantly in the apo
455 and holo states, and were on average larger in the substrate-bound state, consistent with
456 variations also implied by the cryo-EM structures of γ-secretase.[Bai et al., 2015a; Zhou et al.,
457 2019] Equally, the distance between Leu121 and Asp257 of PS1 was on average longer in the
458 C83-bound state, in particular for one conformation (blue trajectory in **Figure S18**).
459

460 **Functionally important dynamics of APH-1B-γ-secretase**

461 To understand the functionally relevant motions of γ-secretase with APH-1B, we measured the
462 Cα-Cα distance between terminal end residues of the substrate gating loop HL1, the distance
463 between the catalytic Asp257 and Asp385 residues of PS1, and the PAL motif terminal residue
464 distance (**Table S4**). The apo states displayed HL1 distances above 2 nm and in some cases
465 close to 3 nm, whereas the holo states displayed more compact HL1 conformations with
466 distances below 2 nm (**Figure S19A**). The motions are arguably the basis for the static ordering
467 of these parts of the protein upon binding to substrates seen in the cryo-EM data.[Yang et al.,
468 2019; Zhou et al., 2019]
469 PS1 can adopt distinct states with the catalytic Asp257 and Asp385 either relatively close
470 or somewhat farther apart, i.e., closed, semi-open and open states of γ-secretase.[Aguayo-Ortiz
471 et al., 2017; Dehury et al., 2019b; Hitzenberger and Zacharias, 2019b] These states can explain
472 C83 processing and the production of different types of Aβ, according to the FIST (fit-induce-
473 stay-trim) model,[Somavarapu and Kepp, 2017; Tang et al., 2018] where the semi-open state is
474 innocent and most active, the closed state does not fit the substrate and is inactive, and the open

475 state gives imprecise cleavage, diverse products, and less activity due to lower substrate
476 affinity and earlier release, i.e. looser “grapping” by the “fist”. This open state is argued to be
477 favored by pathogenic PS1 mutations by destabilizing the membrane protein’s hydrophobic
478 packing,[Mehra and Kepp, 2019; Somavarapu and Kepp, 2016, 2017] explaining their lower
479 activity and higher $A\beta_{42}/A\beta_{40}$ ratios in assays.[Sun et al., 2016] In contrast, γ-secretase
480 modulators may contribute their binding affinity to stabilize the enzyme-substrate-modulator
481 complex, increase substrate residence time, trimming, and production of shorter Aβ.[Tang et
482 al., 2018]

483 We found that protonation of Asp257 in APH-1B-apo-γ-secretase produced a short Asp-
484 Asp distance (~9.2 Å; vs. 8.0 Å in 5FN2) whereas for C83-bound APH-1B-γ-secretase it
485 averaged to ~10.4 Å, comparing well to the experimental 6IYC (10.6 Å). In the obtained open
486 state the distance averages to 1.2 nm with a broader Asp-Asp distribution, fully consistent with
487 the previous studies[Dehury et al., 2019a, 2019b; Somavarapu and Kepp, 2017] that led to the
488 structural-dynamic support for the FIST model (**Figure S19B)**.

489 The PAL motif (Pro433-Ala434-Leu435) in PS1 plays a vital role in substrate
490 recruitment.[Sato et al., 2008] The Cα-Cα distance between Pro433 and Leu435 implied a
491 distinct extension of this motif in the deprotonated apo state as compared to both the apo-γ-
492 secretase with Asp257 protonated and the holo state (**Figure S19C**). Mutation of Leu432
493 affects the PAL motif structure and eliminates the catalytic activity of the enzyme,[Yang et al.,
494 2019; Zhou et al., 2019] and thus the dynamic changes with substrate binding and protonation
495 could be of relevance, although the pH-dependency of γ-secretase is la largely unexplored topic
496 at this point.

497

498 **Dynamics of catalytic aspartate - cleavage site interactions**

499 The distance between the catalytic aspartates of PS1 and the actual cleavage sites of the
500 substrate (in this case C83) is also important to understand the specific cleavage mechanism.

501 We measured the minimum of these distances from the last 300 ns trajectories of the holo
502 states, as summarized in **Figure 6**. The ε-cleavage occurs via two different pathways either at
503 Thr719-Leu720 or at Leu720-Val721 leading to the formation of $A\beta_{48}$ or $A\beta_{49}$.[Bolduc et al.,
504 2016; Wolfe, 2020]. We observed differential distributions in the distance between the catalytic
505 Asp257 and cleavage site residues, with some below 4 Å and some above 8 Å, whereas the
506 distance was generally very short (below 4 Å) in case of Asp385. Thus, the ensembles mainly
507 represent states that are ready to cleave via water binding to Asp385, but later cleavage via
508 Asp257 will then probably occur after loss of the tripeptide fragment.[Bolduc et al., 2016;
509 Takami et al., 2009] The open state arguably enables both of these cleavage pathways to
510 proceed whereas the semi-open state favors the $A\beta_{40}$ pathway.

511 The intermolecular hydrogen-bond dynamics of C83, nicastrin and PS1 (**Figure S20**)
512 indicate a distinct interaction between C83 and PS1 in simulation 3, with a higher number of
513 hydrogen bonds typical of the more compact semi-open state of γ-secretase. We also measured
514 the hydrogen bonds formed between C83 with the lipid molecules and water molecules in each
515 trajectory of the substrate bound conformations of γ-secretase complex (**Figure S20**). A well-
516 positioned water molecule near the two aspartates is required to cleave the substrate.[Singh et
517 al., 2009] As evident from **Figure S20**, fewer hydrogen bonds are formed between lipids and
518 C83, while, ~44 hydrogen bonds existed between C83 and water (**Figure S20**). We observed
519 different accessibility of water to the substrate in the three simulations (~50 in simulation 1,
520 ~70 in simulation 2, and ~26 in simulation 3) by the catalytic aspartates in each C83-bound γ-
521 secretase state (**Figure S20**). These differences may be attributed to the distinct binding states,
522 with the more open state enabling more water molecules to access the catalytic site. To
523 understand the interaction of C83 by γ-secretase with APH-1B, we computed the
524 intermolecular contacts of the structural ensembles obtained from clustering analysis (**Table
525 S5**). In simulation 1, we observed most hydrogen bonds and least in the case of simulation 3. A
526 number of residues in the loop bridging TM6a and the strand β1 interacted consistently with

527 the positively charged triplet lysine anchor motif in C83, consistent with the known role of this
528 polybasic region in anchoring substrate molecules[Xu et al., 2016]. We also found several
529 electrostatic interactions that aid the positioning of the substrates inside the pocket of catalytic
530 PS1.[Yan et al., 2017]
531
532 **Differences between γ-secretase with APH-1A and APH-1B**
533 The most important question of our work is arguably whether, and if so, how, APH-1B affects
534 γ-secretase differently than APH-1A, in particular in relation to the catalytic PS1 subunit. To
535 understand this, we measured the deviations in the TM tilt angles of PS1 and APH-1B. We
536 compared the present data to the MD data of C83 bound γ-secretase with APH-1A subunit
537 from our recently published study[Mehra et al., 2020] that used similar setup, making the two
538 studies directly comparable. We observed surprising differences in PS1 and APH-1B in the apo
539 deprotonated-state (**Figure S21**): The distributions of the tilt angles in TM2, TM3 and TM6 of
540 PS1 differed notably between the APH-1A and APH-1B systems. With APH-1B, TM2, TM3
541 and TM5 of PS1 varied substantially in apo-γ-secretase, whereas the C83-bound γ-secretase
542 with APH-1A and APH-1B differed in terms of TM2, TM3, TM5 and TM6 (**Figure 7**). These
543 differences indicate that APH-1A and APH-1B could favor the open, closed, and semi-open
544 states of PS1 differently, which would affect activity.[Somavarapu and Kepp, 2017]
545 A recent MD study has shown that APH-1A (inside γ-secretase complex: 5FN3) can act as
546 a channel apart from providing stability to γ-secretase complex.[Aguayo-Ortiz and Dominguez,
547 2019] The trajectories obtained in the present work also identify a very persistent channel
548 architecture of APH-1B (**Figures S22-S23**) with many events of water molecules crossing the
549 bilayer near TM3, TM4, TM5 and TM6 of APH-1B. In this respect, the two homologous
550 proteins thus appear similar.
551
552

Conclusions

The intramembrane aspartyl protease complex γ-secretase, containing nicastrin, PEN-2, PS1/PS2, and APH-1A/1B, plays a major role in AD and actively cleaves more than a hundred membrane-bound helical substrates, including C99 to produce the infamous Aβ peptides of variable length. Although all structural and computational work has focused so far on γ-secretase with APH-1A, different γ-secretase complexes containing APH-1A or APH1-B subunits display heterogeneous biochemical and physiological properties.[Araki et al., 2006; Serneels et al., 2009] APH-1A/B interacts with presenilin and affects the processing of substrates, thus modulating the $A\beta_{42}/A\beta_{40}$ ratio.[Acx et al., 2014; Lessard et al., 2015] Accordingly, it is important to understand the structure and dynamics also of γ-secretase with the APH-1B subunit, which was the aim of the present work.

From our simulated homology models of APH-1B alone and in complex with γ-secretase both with and without substrate (C83) bound, we find that APH-1B resembles APH-1A in its ability to transport waters across the bilayer and adopting the same 7TM topology with minor variation in the JM helix at the C-terminal end. The water molecules inside the APH-1B cavity formed interactions with several polar residues including notably Glu84, Arg87, His170, and His196. The conserved histidines His170 and His196 have been implicated to play decisive role in water transportation across the bilayer in APH-1A in previous work, and our work on APH-1B supports these findings.[Aguayo-Ortiz and Dominguez, 2019] Further studies seem necessary to understand the role of the water-containing cavity in APH-1 in the context of the proteolytic activity of γ-secretase.

We conducted multiple all-atom MD simulations of γ-secretase with APH-1B subunit in a complete POPC lipid bilayer to understand the physiological temperature membrane dynamics of the protein complex, using the cryo-EM structures as templates.[Bai et al., 2015a; Zhou et al., 2019] Our structures after equilibration are in excellent agreement with the experimental

579 structures both differ in some parts of APH-1B which also mostly correlate with major
580 sequence variations in the two homologous forms of APH-1A/B. We observed that the
581 protonation of the catalytic aspartates of PS1 affect the distance between the aspartates and the
582 size of the catalytic pocket, which could potentially affect substrate cleavage, although the pH-
583 dependency of γ-secretase activity has not yet been studied to our knowledge. Fluorescence
584 lifetime imaging indicates that PS1 becomes more compact upon binding to APH-1B compared
585 to APH-1A.[Serneels et al., 2009] Our dynamic ensembles support these findings and trace
586 them to differences in the loops and TM helices.

587 The accessibility of water molecules to the catalytic aspartates of PS1 was monitored by
588 calculating the water molecules near the site along the trajectories. Many water molecules
589 access the active site during the normal membrane dynamics, but the access is strongly
590 regulated by the conformational states of the enzyme, and we notably see both open and
591 compact states with respect to catalytic pocket size, controlled by the PS1 TMs, consistent with
592 our previous findings for γ-secretase with APH-1A that underlie the FIST model.[Somavarapu
593 and Kepp, 2016, 2017; Tang et al., 2018] APH-1B was markedly less structurally variable in
594 the C83-bound state compared to the apo states, i.e. substrate binding dampens the motion of
595 APH-1B in the same way as seen for APH-1A.

596 A notable difference between APH-1A and APH-1B, apart from the substantial dynamic
597 differences in the loops where the sequences differ most, was the distribution of TM tilt angles
598 in the apo and substrate-bound states, indicating different effect on the conformational states
599 and perhaps stability of γ-secretase for the two APH-1 forms. In particular, we find that the
600 typical distance between the catalytic aspartates of PS1 and the C83 cleavage sites are shorter
601 in APH-1B, i.e. it represents a more closed state, due to interactions with the C-terminal
602 fragment of PS1. Since both forms of γ-secretase occur physiologically, our findings should be
603 important when understanding the physiological activity of the enzyme complex and when
604 targeting it to modulate Aβ production as widely sought as a major AD drug strategy.

605

606 **Supporting information**

607 The data required to reproduce the present computational work and scrutinize details of the
608 analysis are included in the file named "suppinfo.pdf". Furthermore, the full representative
609 structures from cluster analysis are available as PDB files for each independent simulation.

610

611 **Competing interests statement**

612 All authors hereby declare that they have no competing interests, neither financial nor non-
613 financial, related to this work.

614

615 **Data availability statement**

616 The data that supports the findings of this study are available in the supplementary material of
617 this article. Additional raw data (trajectory files, representative structures) are available from
618 the authors upon reasonable request.

619

620 **References**

621 Abraham MJ, Murtola T, Schulz R, Páll S, Smith JC, Hess B, Lindah E. 2015. Gromacs: High
622 performance molecular simulations through multi-level parallelism from laptops to
623 supercomputers. SoftwareX 1–2:19–25.
624 Acx H, Chávez-Gutiérrez L, Serneels L, Lismont S, Benurwar M, Elad N, Strooper B De.
625 2014. Signature Amyloid β Profiles Are Produced by Different γ-Secretase Complexes. J Biol
626 Chem 289(7):4346–4355.
627 Aguayo-Ortiz R, Chávez-García C, Straub JE, Dominguez L. 2017. Characterizing the
628 structural ensemble of γ-secretase using a multiscale molecular dynamics approach. Chem Sci
629 8(8):5576–5584.

630 Aguayo-Ortiz R, Dominguez L. 2018. Simulating the γ-secretase enzyme: Recent advances and
631 future directions. Biochimie 147:130–135.
632 Aguayo-Ortiz R, Dominguez L. 2019. APH-1A component of γ-secretase forms an internal
633 water and ion-containing cavity. ACS Chem Neurosci 10(6):2931–2938.
634 Aguayo-Ortiz R, Straub JE, Dominguez L. 2018. Influence of membrane lipid composition on
635 the structure and activity of γ-secretase. Phys Chem Chem Phys 20(43):27294–27304.
636 Altschul S, Madden T, Schaffer A, Zhang J, Zhang Z, Miller W, Lipman D. 1997. Gapped
637 BLAST and PSI-BLAST: a new generation of protein database search programs. Nucleic Acids
638 Res 25.
639 Angel TE, Chance MR, Palczewski K. 2009. Conserved waters mediate structural and
640 functional activation of family A (rhodopsin-like) G protein-coupled receptors. Proc Natl Acad
641 Sci 106(21):8555–8560.
642 Araki W, Saito S, Takahashi-Sasaki N, Shiraishi H, Komano H, Murayama KS. 2006.
643 Characterization of APH-1 mutants with a disrupted transmembrane GxxxG motif. J Mol
644 Neurosci 29(1):35–43.
645 Bai X, Rajendra E, Yang G, Shi Y, Scheres SH. 2015a. Sampling the conformational space of
646 the catalytic subunit of human γ-secretase. Elife 4:551–560.
647 Bai X, Yan C, Yang G, Lu P, Sun L, Zhou R, Scheres SHW, Shi Y. 2015b. An atomic structure
648 of human γ-secretase. Nature 525:212–218.
649 Blennow K, Leon MJ de, Zetterberg H. 2015. Alzheimer's disease. Lancet 368(9533):387–403.
650 Bogdanov M, Mileykovskaya E, Dowhan W. 2008. Lipids in the assembly of membrane
651 proteins and organization of protein supercomplexes: implications for lipid-linked disorders.
652 Lipids in Health and Disease. Springer. p 197–239.
653 Bolduc DM, Montagna DR, Seghers MC, Wolfe MS, Selkoe DJ. 2016. The amyloid-beta
654 forming tripeptide cleavage mechanism of γ-secretase. Elife 5:e17578.
655 Bondar A-N, White SH. 2012. Hydrogen bond dynamics in membrane protein function.

656 Biochim Biophys Acta (BBA)-Biomembranes 1818(4):942–950.
657 Buchoux S. 2017. FATSLiM: A fast and robust software to analyze MD simulations of
658 membranes. Bioinformatics 33(1):133–134.
659 Cai T, Yonaga M, Tomita T. 2017. Activation of γ-secretase trimming activity by topological
660 changes of transmembrane domain 1 of presenilin 1. J Neurosci 37(50):12272–12280.
661 Caldararu O, Kumar R, Oksanen E, Logan DT, Ryde U. 2019. Are crystallographic B-factors
662 suitable for calculating protein conformational entropy? Phys Chem Chem Phys 21(33):18149–
663 18160.
664 Chen VB, Arendall WB, Headd JJ, Keedy DA, Immormino RM, Kapral GJ, Murray LW,
665 Richardson JS, Richardson DC. 2010. MolProbity: All-atom structure validation for
666 macromolecular crystallography. Acta Crystallogr D 66(1):12–21.
667 Cheung T, Younkin S, Suzuki N, Otvos L, Eckman C, Cai X, Odaka A, Golde T. 2006. An
668 increased percentage of long amyloid beta protein secreted by familial amyloid beta protein
669 precursor (beta APP717) mutants. Science (80-) 264(5163):1336–1340.
670 Colovos C, Yeates TO. 1993. Verification of protein structures: Patterns of nonbonded atomic
671 interactions. Protein Sci 2(9):1511–1519.
672 Coolen MW, Loo KMJ van, Bakel NNHM van, Ellenbroek BA, Cools AR, Martens GJM.
673 2006. Reduced Aph-1b expression causes tissue-and substrate-specific changes in γ-secretase
674 activity in rats with a complex phenotype. FASEB J 20(1):175–177.
675 Corradi V, Sejdiu BI, Mesa-Galloso H, Abdizadeh H, Noskov SY, Marrink SJ, Tieleman DP.
676 2019. Emerging diversity in lipid–protein interactions. Chem Rev 119(9):5775–5848.
677 Crump CJ, Johnson DS, Li YM. 2013. Development and mechanism of γ-secretase modulators
678 for Alzheimer's disease. Biochemistry 52(19):3197–3216.
679 Dehury B, Tang N, Blundell TL, Kepp KP. 2019a. Structure and dynamics of γ-secretase with
680 presenilin 2 compared to presenilin 1. RSC Adv 9(36):20901–20916.
681 Dehury B, Tang N, Kepp KP. 2019b. Molecular dynamics of C99-bound γ-secretase reveal two

682 binding modes with distinct compactness, stability, and active-site retention: Implications for
683 Aβ production. Biochem J 476(7):1173–1189.
684 Dehury B, Tang N, Kepp KP. 2019c. Insights into membrane-bound presenilin 2 from all-atom
685 molecular dynamics simulations. J Biomol Struct Dyn 1–15.
686 Dejaegere T, Serneels L, Schäfer MK, Biervliet J Van, Horré K, Depboylu C, Alvarez-Fischer
687 D, Herreman A, Willem M, Haass C. 2008. Deficiency of Aph1B/C-γ-secretase disturbs Nrg1
688 cleavage and sensorimotor gating that can be reversed with antipsychotic treatment. Proc Natl
689 Acad Sci 105(28):9775–9780.
690 Dominguez L, Foster L, Straub JE, Thirumalai D. 2016. Impact of membrane lipid composition
691 on the structure and stability of the transmembrane domain of amyloid precursor protein. Proc
692 Natl Acad Sci 113(36):E5281–E5287.
693 Elad N, Strooper B De, Lismont S, Hagen W, Veugelen S, Arimon M, Horré K, Berezovska O,
694 Sachse C, Chávez-Gutiérrez L. 2015. The dynamic conformational landscape of γ-secretase. J
695 Cell Sci 128(3):589–598.
696 Esch FS, Keim PS, Beattie EC, Blacher RW, Culwell AR, Oltersdorf T, McClure D, Ward PJ.
697 1990. Cleavage of amyloid beta peptide during constitutive processing of its precursor. Science
698 (80-) 248(4959):1122–1124.
699 Fazzari P, Snellinx A, Sabanov V, Ahmed T, Serneels L, Gartner A, Shariati SAM, Balschun
700 D, Strooper B De. 2014. Cell autonomous regulation of hippocampal circuitry via Aph1b-γ-
701 secretase/neuregulin 1 signalling. Elife 3:e02196.
702 Francis R, McGrath G, Zhang J, Ruddy DA, Sym M, Apfeld J, Nicoll M, Maxwell M, Hai B,
703 Ellis MC, Parks AL, Xu W, Li J, Gurney M, Myers RL, Himes CS, Hiebsch R, Ruble C, Nye
704 JS, Curtis D. 2002. aph-1 and pen-2 are required for Notch pathway signaling, γ-secretase
705 cleavage of βAPP, and presenilin protein accumulation. Dev Cell 3:85–97.
706 Fukumori A, Steiner H. 2016. Substrate recruitment of γ-secretase and mechanism of clinical
707 presenilin mutations revealed by photoaffinity mapping. EMBO J e201694151.

708 Golde TE, Estus S, Younkin LH, Selkoe DJ, Younkin SG. 1992. Processing of the amyloid
709 protein precursor to potentially amyloidogenic derivatives. Science (80-) 255(5045):728–730.
710 Golde TE, Koo EH, Felsenstein KM, Osborne BA, Miele L. 2013. γ-Secretase inhibitors and
711 modulators. Biochim Biophys Acta - Biomembr 1828(12):2898–2907.
712 Goutte C, Tsunozaki M, Hale VA, Priess JR. 2002. APH-1 is a multipass membrane protein
713 essential for the Notch signaling pathway in Caenorhabditis elegans embryos. Proc Natl Acad
714 Sci 99(2):775–779.
715 Gu Y, Chen F, Sanjo N, Kawarai T, Hasegawa H, Duthie M, Li W, Ruan X, Luthra A, Mount
716 HTJ. 2003. APH-1 interacts with mature and immature forms of presenilins and nicastrin and
717 may play a role in maturation of presenilin· nicastrin complexes. J Biol Chem 278(9):7374–
718 7380.
719 Haapasalo A, Kovacs DM. 2011. The many substrates of presenilin/γ-secretase. J Alzheimer's
720 Dis 25:3–28.
721 Hardy JA, Higgins GA. 1992. Alzheimer's disease: the amyloid cascade hypothesis. Science
722 (80-) 256(5054):184–185.
723 Hekkelman ML, Beek TAH te, Pettifer SR, Thorne D, Attwood TK, Vriend G. 2010. WIWS:
724 A protein structure bioinformatics web service collection. Nucleic Acids Res 38(SUPPL.
725 2):719–723.
726 Heo L, Park H, Seok C. 2013. GalaxyRefine: Protein structure refinement driven by side-chain
727 repacking. Nucleic Acids Res 41(Web Server issue):W384–W388.
728 Hitzenberger M, Zacharias M. 2019a. Structural Modeling of γ-Secretase Aβ n Complex
729 Formation and Substrate Processing. ACS Chem Neurosci acschemneuro.8b00725.
730 Hitzenberger M, Zacharias M. 2019b. γ-Secretase Studied by Atomistic Molecular Dynamics
731 Simulations: Global Dynamics, Enzyme Activation, Water Distribution and Lipid Binding.
732 Front Chem 6:640.
733 Holmes O, Paturi S, Ye W, Wolfe MS, Selkoe DJ. 2012. Effects of membrane lipids on the

734 activity and processivity of purified γ-secretase. Biochemistry 51(17):3565–3575.
735 Huang J, Rauscher S, Nawrocki G, Ran T, Feig M, Groot BL De, Grubmüller H, MacKerell
736 AD. 2016. CHARMM36m: An improved force field for folded and intrinsically disordered
737 proteins. Nat Methods 14(1):71–73.
738 Imbimbo BP, Giardina GAM. 2011. gamma-secretase inhibitors and modulators for the
739 treatment of Alzheimer's disease: disappointments and hopes. Curr Top Med Chem
740 11(12):1555–1570.
741 Jo S, Kim T, Iyer VG, Im W. 2008. CHARMM-GUI: A web-based grraphical user interface for
742 CHARMM. J Comput Chem 29(11):1859–1865.
743 Julia TCW, Goate AM. 2017. Genetics of β-amyloid precursor protein in Alzheimer's Disease.
744 Cold Spring Harb Perspect Med 7(6):a024539.
745 Kepp KP. 2016. Alzheimer's disease due to loss of function: A new synthesis of the available
746 data. Prog Neurobiol 143:36–60.
747 Kepp KP. 2017. Ten Challenges of the Amyloid Hypothesis of Alzheimer's Disease. J
748 Alzheimer's Dis 55(2):447–457.
749 Kimberly WT, LaVoie MJ, Ostaszewski BL, Ye W, Wolfe MS, Selkoe DJ. 2003. Gamma-
750 secretase is a membrane protein complex comprised of presenilin, nicastrin, Aph-1, and Pen-2.
751 Proc Natl Acad Sci U S A 100:6382–6387.
752 Kong R, Chang S, Xia W, Wong STC. 2015. Molecular dynamics simulation study reveals
753 potential substrate entry path into gamma-secretase/presenilin-1. J Struct Biol 191(2):120–129.
754 Laskowski RA, MacArthur MW, Moss DS, Thornton JM. 1993. PROCHECK: a program to
755 check the stereochemical quality of protein structures. J Appl Crystallogr 26(2):283–291.
756 Lee H, Casadesus G, Zhu X, Takeda A, Perry G, Smith MA. 2004a. Challenging the amyloid
757 cascade hypothesis: Senile plaques and amyloid-β as protective adaptations to Alzheimer
758 disease. Ann N Y Acad Sci 1019(1):1–4.
759 Lee JY, Feng Z, Xie XQ, Bahar I. 2017. Allosteric Modulation of Intact γ-Secretase Structural

760 Dynamics. Biophys J 113(12):2634–2649.
761 Lee S-F, Shah S, Li H, Yu C, Han W, Yu G. 2002. Mammalian APH-1 interacts with
762 presenilin and nicastrin and is required for intramembrane proteolysis of amyloid-β precursor
763 protein and Notch. J Biol Chem 277(47):45013–45019.
764 Lee S-F, Shah S, Yu C, Wigley WC, Li H, Lim M, Pedersen K, Han W, Thomas P, Lundkvist
765 J. 2004b. A conserved GXXXG motif in APH-1 is critical for assembly and activity of the γ-
766 secretase complex. J Biol Chem 279(6):4144–4152.
767 Lee Y, Kim S, Choi S, Hyeon C. 2016. Ultraslow water-mediated transmembrane interactions
768 regulate the activation of A2A adenosine receptor. Biophys J 111(6):1180–1191.
769 Lessard CB, Cottrell BA, Maruyama H, Suresh S, Golde TE, Koo EH. 2015. γ-secretase
770 modulators and APH1 isoforms modulate γ-secretase cleavage but not position of ε-cleavage of
771 the amyloid precursor protein (APP). PLoS One 10(12):e0144758.
772 Lomize AL, Pogozheva ID, Lomize MA, Mosberg HI. 2006. Positioning of proteins in
773 membranes: A computational approach. Protein Sci 15(6):1318–1333.
774 Lomize MA, Pogozheva ID, Joo H, Mosberg HI, Lomize AL. 2012. OPM database and PPM
775 web server: Resources for positioning of proteins in membranes. Nucleic Acids Res
776 40(D1):D370–D376.
777 Lüthy R, Bowie JU, Eisenberg D. 1992. Assessment of protein models with three-dimensional
778 profiles. Nature 356(6364):83–85.
779 Luukkainen L, Helisalmi S, Kytövuori L, Ahmasalo R, Solje E, Haapasalo A, Hiltunen M,
780 Remes AM, Krüger J. 2019. Mutation Analysis of the Genes Linked to Early Onset
781 Alzheimer's Disease and Frontotemporal Lobar Degeneration. J Alzheimer's Dis (Preprint):1–
782 8.
783 Lyubartsev AP, Rabinovich AL. 2016. Force Field Development for Lipid Membrane
784 Simulations. Biochim Biophys Acta - Biomembr 1858(10):2483–2497.
785 Mehra R, Dehury B, Kepp KP. 2020. Cryo-temperature effects on membrane protein structure

786 and dynamics. Phys Chem Chem Phys in press.
787 Mehra R, Kepp KP. 2019. Computational analysis of Alzheimer-causing mutations in amyloid
788 precursor protein and presenilin 1. Arch Biochem Biophys 678:108168.
789 Ng HW, Laughton CA, Doughty SW. 2014. Molecular Dynamics Simulations of the
790 Adenosine A2a Receptor in POPC and POPE Lipid Bilayers: Effects of Membrane on Protein
791 Behavior. J Chem Inf Model 54(2):573–581.
792 Osenkowski P, Ye W, Wang R, Wolfe MS, Selkoe DJ. 2008. Direct and potent regulation of γ-
793 secretase by its lipid microenvironment. J Biol Chem 283(33):22529–22540.
794 Pauwels K, Williams TL, Morris KL, Jonckheere W, Vandersteen A, Kelly G, Schymkowitz J,
795 Rousseau F, Pastore A, Serpell LC, Broersen K. 2012. Structural basis for increased toxicity of
796 pathological aβ42:aβ40 ratios in Alzheimer disease. J Biol Chem 287(8):5650–5660.
797 Petit D, Hitzenberger M, Lismont S, Zoltowska KM, Ryan NS, Mercken M, Bischoff F,
798 Zacharias M, Chávez-Gutiérrez L. 2019. Extracellular interface between APP and Nicastrin
799 regulates Aβ length and response to γ-secretase modulators. EMBO J 38(12).
800 Sato C, Takagi S, Tomita T, Iwatsubo T. 2008. The C-Terminal PAL Motif and
801 Transmembrane Domain 9 of Presenilin 1 Are Involved in the Formation of the Catalytic Pore
802 of the γ-Secretase. J Neurosci 28(24):6264–6271.
803 Sato T, Diehl TS, Narayanan S, Funamoto S, Ihara Y, Strooper B De, Steiner H, Haass C,
804 Wolfe MS. 2007. Active γ-secretase complexes contain only one of each component. J Biol
805 Chem 282(47):33985–33993.
806 Selkoe DJ, Hardy J. 2016. The amyloid hypothesis of Alzheimer's disease at 25 years. EMBO
807 Mol Med 8(6):595–608.
808 Serneels L, Biervliet J Van, Craessaerts K, Dejaegere T, Horré K, Houtvin T Van, Esselmann
809 H, Paul S, Schäfer MK, Berezovska O. 2009. γ-Secretase heterogeneity in the Aph1 subunit:
810 Relevance for Alzheimer's disease. Science (80-) 324(5927):639–642.
811 Shen J, Kelleher RJ. 2007. The presenilin hypothesis of Alzheimer's disease: evidence for a

812 loss-of-function pathogenic mechanism. Proc Natl Acad Sci U S A 104(2):403–409.
813 Shirotani K, Edbauer D, Prokop S, Haass C, Steiner H. 2004. Identification of distinct γ-
814 secretase complexes with different APH-1 variants. J Biol Chem 279(40):41340–41345.
815 Singh R, Barman A, Prabhakar R. 2009. Computational insights into aspartyl protease activity
816 of presenilin 1 (ps1) generating alzheimer amyloid β-peptides (aβ40 and aβ42). J Phys Chem B
817 113(10):2990–2999.
818 Smith MA, Casadesus G, Joseph JA, Perry G. 2002. Amyloid-β and τ serve antioxidant
819 functions in the aging and Alzheimer brain. Free Radic Biol Med 33(9):1194–1199.
820 Somavarapu AK, Kepp KP. 2016. Loss of stability and hydrophobicity of presenilin 1
821 mutations causing Alzheimer's Disease. J Neurochem 137:101–111.
822 Somavarapu AK, Kepp KP. 2017. Membrane Dynamics of γ-Secretase Provides a Molecular
823 Basis for β-Amyloid Binding and Processing. ACS Chem Neurosci 8(11):2424–2436.
824 Sun L, Zhao L, Yang G, Yan C, Zhou R, Zhou X, Xie T, Zhao Y, Wu S, Li X, Shi Y. 2015.
825 Structural basis of human γ-secretase assembly. Proc Natl Acad Sci U S A 112(19):6003–6008.
826 Sun L, Zhou R, Yang G, Shi Y. 2016. Analysis of 138 pathogenic mutations in presenilin-1 on
827 the in vitro production of Aβ42 and Aβ40 peptides by γ-secretase. Proc Natl Acad Sci
828 114(4):E476–E485.
829 Sun Z, Liu Q, Qu G, Feng Y, Reetz MT. 2019. Utility of B-factors in protein science:
830 interpreting rigidity, flexibility, and internal motion and engineering thermostability. Chem
831 Rev 119(3):1626–1665.
832 Szaruga M, Munteanu B, Lismont S, Veugelen S, Horré K, Mercken M, Saido TC, Ryan NS,
833 Vos T De, Savvides SN, Gallardo R, Schymkowitz J, Rousseau F, Fox NC, Hopf C, Strooper B
834 De. 2017. Alzheimer's-Causing Mutations Shift Aβ Length by Destabilizing γ-Secretase-Aβn
835 Interactions. Cell 170(3):443–456.
836 Takagi-Niidome S, Sasaki T, Osawa S, Sato T, Morishima K, Cai T, Iwatsubo T, Tomita T.
837 2015. Cooperative Roles of Hydrophilic Loop 1 and the C-Terminus of Presenilin 1 in the

838 Substrate-Gating Mechanism of γ-Secretase. J Neurosci 35(6):2646–2656.
839 Takami M, Nagashima Y, Sano Y, Ishihara S, Morishima-Kawashima M, Funamoto S, Ihara
840 Y. 2009. γ-Secretase: successive tripeptide and tetrapeptide release from the transmembrane
841 domain of β-carboxyl terminal fragment. J Neurosci 29(41):13042–13052.
842 Tang N, Kepp KP. 2018. Aβ42/Aβ40 ratios of presenilin 1 mutations correlate with clinical
843 onset of Alzheimer's disease. J Alzheimer's Dis 66(3):939–945.
844 Tang N, Somavarapu AK, Kepp KP. 2018. Molecular Recipe for γ-Secretase Modulation from
845 Computational Analysis of 60 Active Compounds. ACS Omega 3(12):18078–18088.
846 Tomobe K, Yamamoto E, Kholmurodov K, Yasuoka K. 2017. Water permeation through the
847 internal water pathway in activated GPCR rhodopsin. PLoS One 12(5).
848 Vassar R, Bennett BD, Babu-Khan S, Kahn S, Mendiaz EA, Denis P, Teplow DB, Ross S,
849 Amarante P, Loeloff R, Luo Y, Fisher S, Fuller J, Edenson S, Lile J, Jarosinski MA, Biere AL,
850 Curran E, Burgess T, Louis JC, Collins F, Treanor J, Rogers G, Citron M. 1999. Beta-secretase
851 cleavage of Alzheimer's amyloid precursor protein by the transmembrane aspartic protease
852 BACE. Science 286(5440):735–741.
853 Webb B, Sali A. 2017. Protein structure modeling with MODELLER. Methods in Molecular
854 Biology. Humana Press, New York, NY. p 39–54.
855 Winkler E, Kamp F, Scheuring J, Ebke A, Fukumori A, Steiner H. 2012. Generation of
856 Alzheimer disease-associated amyloid β42/43 peptide by γ-secretase can be inhibited directly
857 by modulation of membrane thickness. J Biol Chem 287(25):21326–34.
858 Wolfe MS. 2020. Unraveling the complexity of γ-secretase.
859 Xu TH, Yan Y, Kang Y, Jiang Y, Melcher K, Xu HE. 2016. Alzheimer's disease-associated
860 mutations increase amyloid precursor protein resistance to γ-secretase cleavage and the
861 Aβ42/Aβ40 ratio. Cell Discov 2:16026.
862 Yan Y, Xu TH, Melcher K, Xu HE. 2017. Defining the minimum substrate and charge
863 recognition model of gamma-secretase. Acta Pharmacol Sin 38(10):1412–1424.

864 Yang G, Zhou R, Zhou Q, Guo X, Yan C, Ke M, Lei J, Shi Y. 2019. Structural basis of Notch
865 recognition by human γ-secretase. Nature 565(7738):192–197.
866 Zhou R, Yang G, Guo X, Zhou Q, Lei J, Shi Y. 2019. Recognition of the amyloid precursor
867 protein by human γ-secretase. Science (80-) 363(6428):eaaw0930.
868 Zhuang X, Dávila-Contreras EM, Beaven AH, Im W, Klauda JB. 2016. An extensive
869 simulation study of lipid bilayer properties with different head groups, acyl chain lengths, and
870 chain saturations. Biochim Biophys Acta - Biomembr 1858(12):3093–3104.
871 Zhuang X, Makover JR, Im W, Klauda JB. 2014. A systematic molecular dynamics simulation
872 study of temperature dependent bilayer structural properties. Biochim Biophys Acta -
873 Biomembr 1838(10):2520–2529.
874
875

876 **Figure legends**

877

878 **Figure 1**. **Sequence and structural comparison of APH-1 subunits (APH-1 and APH1-B)**
879 **of γ-Secretase.** (**A**) Sequence alignment of APH-1A (265 aa) and APH-1B (257 aa). The
880 transmembrane helix region is marked by cyan encirclement and the GxxxG motif is marked
881 with stars. (**B**) Ramchandran analysis of modelled APH-1B with 97.8% of residues in the most
882 allowed region. (**C**) The overall 7TM architecture of APH-1B (conserved regions are shown in
883 red and variable regions in white). (**D**) Structural overlay of our modelled APH-1B subunit
884 (green) with the APH-1A subunits from cryo-EM structures (5FN2: light blue, 5A63: magenta
885 and 6IYC: yellow), with the GxxxG motif encircled. The C-α RMSD of APH-1B with respect
886 to APH-1A of 5FN2, 5FN3 and 6IYC are 0.47, 0.37, and 0.46 Å, respectively.

887

888 **Figure 2**. **Structural dynamics of APH-1B alone in a lipid bilayer.** (**A**) Backbone RMSD of
889 triplicate APH-1B simulations. Blue, orange and cyan lines represent simulation 1, 2, and 3.
890 (**B**) Cα-RMSF for each residue of APH-1B during the last 300 ns MD. The B-factors with the
891 flipping regions are shown in putty format to the right, using PyMOL. (**C**) Experimental APH-
892 1A from 5FN2 (green) superimposed with representative structures for simulation 1 (blue), 2
893 (orange), and 3 (cyan).

894

895 **Figure 3. Simulated γ-secretase models with APH-1B in a lipid bilayer with zoomed view**
896 **of catalytic aspartates**. (**A**) Apo-γ-secretase with APH-1B (with deprotonated Asp257 and
897 Asp385) and the backbone RMSD of the complex simulations. (**B**) Apo-γ-secretase with
898 protonated Asp257 with APH-1B and the backbone RMSD. (**C**) C83-bound APH-1B-γ-
899 secretase and backbone RMSD. The small colored spheres represent the POPC head groups.
900 Blue, orange and cyan lines represent simulation 1, 2, and 3 of each system.

901

902 **Figure 4**. **Comparison of simulated γ-secretase (with APH-1B subunit and experimental**
903 **cryo-EM structures 5FN2 and 6IYC (with APH-1A)**. (**A**) Superimposed view of the
904 representative structures of apo-γ-secretase (deprotonated Asp257 and Asp385) with that of
905 experimental 5FN2 structures. **(B)** Superimposed view of the representative simulated
906 structures of C83-bound γ-secretase with APH-1B and experimental 6IYC (with APH-1A).
907 The blue, orange and cyan colors represent simulation 1, 2, and 3; the experimental cryo-EM
908 structures are shown in green.

909

910 **Figure 5**. **Cα RMSF analysis of each subunit of apo and holo states of γ-secretase with**
911 **APH-1B.** The blue, orange, and cyan lines represent the RMSF for Cα-atoms of each subunit
912 from simulations 1, 2, and 3. **Upper Panel**: Cα-RMSF of Nicastrin, PS1, APH-1B and PEN2
913 in apo-γ-secretase with deprotonated Asp257 and Asp385 of PS1. **Middle Panel**: Cα-RMSF of
914 Nicastrin, PS1, APH-1B and PEN2 in apo-γ-secretase system with protonated Asp257. **Lower**
915 **Panel**: Cα-RMSF of Nicastrin, PS1, APH-1B, and PEN2 in C83-bound γ-secretase.

916

917 **Figure 6. Distances between catalytic Asp257/Asp385 and C83 cleavage sites in γ-**
918 **secretase with APH-1B**. The distances shown are those between the two catalytic residues of
919 PS1 and the cleavage sites Leu720-Val721 and Thr719-Leu720, computed using the *gmx*
920 *mindist* utility toolkit from the last 300 ns of each trajectory.

921

922 **Figure 7. Distribution of TM tilt angles of PS1 and APH1 in γ-secretase with APH-1A and**
923 **APH-1B.** The tilt angles of PS1/APH-1A are from our previous study.[Mehra et al., 2020] The
924 tilt angles were computed using the Cα coordinates of the TMs. **Left Panel**: Comparison of tilt
925 angles of TM helices of PS1 in γ-secretase-C83 with APH-1A and APH-1B. **Right Panel**:
926 Comparison of TM tilt angles of APH1 subunits in γ-secretase-C83 with APH-1A and APH-
927 1B.